Optical Tomogram of Number State Filtered Coherent States

J. Merlin and A. Basherrudin Mahmud Ahmed*

School of Physics, Madurai Kamaraj University, Madurai 625021, Tamilnadu, India

Received: 30.12.2021 & Accepted: 02.02.2022

Doi: 10.12693/APhysPolA.141.516 *e-mail: abmahmed@gmail.com

The optical tomogram of the number state filtered coherent states is studied comprehensively. The superposition of coherent state and number state is reflected in the optical tomogram via quantum interference. The qualitative signatures of the nonclassicality are captured as rapid oscillations in the optical tomogram of number state filtered coherent states. Entropic squeezing is estimated directly from the optical tomogram through the Shannon information entropy. The effects of the non-unit quantum efficiency of the photodetectors on the optical tomogram and the entropic squeezing are observed. Finally, two decoherence models, namely phase damping and amplitude damping models, are employed to assess the degradation of the nonclassical features in the optical tomogram.

topics: coherent state, state filtration, optical tomogram, entropic squeezing

1. Introduction

The key element needed to describe the physical systems in the quantum realm is the wave function of the system. It contains all the information about the system of interest. The state vector ($|\psi\rangle$) denotes the pure states, whereas the density operator ($\hat{\rho}$) [1] denotes both the pure and mixed states. In addition to these, quasi-probability distributions can be used to represent the system in phase space [2]. Commonly used quasi-probability distributions are the Glauber–Sudarshan P function [3], the Husimi Q function [4], and the Wigner function [5]. Besides them, there is a real probability distribution called optical tomography representing the state of the system [6]. The optical tomogram has a one-to-one correspondence with the quasi-probability distributions [7, 8]. Unlike the quasi-probability distributions, the tomogram is positive and fulfills all the characteristics of the probability distribution function. Indeed, optical tomograms of the continuous variable radiation states can be measured in the laboratory using homodyne detection [9]. This signifies that all the physical characteristics can be extracted from the optical tomogram. Hence one can use the optical tomogram as a primary notion of the system and bypass the reconstruction procedure [10]. Optical homodyne detection is also employed in the characterization of optical devices [11]. Aided by the direct density operator reconstruction schemes without resorting to the Wigner function approach, the experimental detection of nonclassical radiation states from optical tomograms has gained momentum [12]. Theoretical tomographic descriptions of diverse nonclassical states have been studied [13–15]. In contrast, estimation of density operators of finite dimensional quantum systems is also an intense research area [16–19].

Radiation states are generally adopted in quantum state engineering as they can be easily manipulated from classical thermal and coherent states [20]. Several techniques have been reported to generate nonclassical states. Addition [21] and subtraction [22] of photons from classical states are known to exhibit nonclassicality. Experimental realization of the nonclassical states, such as photon-added coherent states (PACS) [23], to the sophisticated manipulation of multiphoton catalysis involving the function of creation and annihilation operators have been achieved. In addition to these, truncation [24, 25] and hole burning [26–28] methods are also employed in generation of nonclassical states. The hole burning or filtration process was recently performed on the coherent states and named as the number state filtered coherent states (NSFS) [29]. It is represented as

$$\big|\psi(\alpha,n)\big\rangle = N_n\Big(\,|\alpha\rangle - C_n\;|n\rangle\,\Big), \tag{1}$$

where $|\alpha\rangle$ ($\alpha = |\alpha|\mathrm{e}^{\mathrm{i}\xi}$) is the coherent state, ξ denotes the phase of the coherent amplitude, $|n\rangle$ is the number state, $C_n = \mathrm{e}^{-|\alpha^2|/2}\frac{\alpha^n}{\sqrt{n!}}$ and $N_n = 1/\sqrt{1-|C_n|^2}$, which is the normalization after filtration. Number state filtration from the coherent state makes the state exhibit excellent nonclassical properties, such as the negativity of the Wigner function. Moreover, filtration of the vacuum state from the coherent state has shown to be more robust than the addition of a photon to the coherence state

in the presence of the noise. Phase sensitivity quantifies the performance of the state in quantum information protocols and has been measured using the quantum Fisher information. NSFS has been observed to show a better phase sensitivity when coherent state and NSFS were used as the inputs of the interferometer [30]. Being a potential nonclassical candidate for quantum metrological applications, NSFS deserves further studies. An interesting aspect to explore is its optical tomogram, since optical tomograms are the equivalent state representation in the experiments. In this work, the distinct features in the optical tomogram of NSFS, the effect of experimental imperfections, and the environmental couplings on the tomogram are investigated.

In the next section, rotated quadrature operator and entropic inequality are expressed. The optical tomogram pattern of NSFS and discussion on the extent of entropic squeezing are presented in Sect. 3. In Sect. 4, the effect of non-ideal photodetectors in the tomogram and entropic squeezing are investigated. The influence of phase damping and amplitude damping models on NSFS is explained in Sect. 5. Finally, the results are concluded in Sect. 6.

2. Rotated quadrature operator and entropic inequality

2.1. Optical tomography

The optical homodyne measurement is performed by measuring the rotated quadrature operator in all possible directions by changing the phase of the local oscillator. The rotated quadrature operator is defined [6, 7] as

$$\hat{X}_\phi = \frac{1}{\sqrt{2}} \left(\hat{a}\, \mathrm{e}^{-\mathrm{i}\,\phi} + \hat{a}^\dagger \mathrm{e}^{\mathrm{i}\,\phi} \right). \tag{2}$$

Here, ϕ denotes the phase of the local oscillator, $\hat{a}^\dagger$ and $\hat{a}$ stand for photonic creation and annihilation operators, respectively. The probability distribution of the quadrature operator is given [6, 9] by

$$\omega(X_\phi, \phi) = \left\langle X_\phi, \phi \middle| \hat{\rho} \middle| X_\phi, \phi \right\rangle, \tag{3}$$

where the eigenstates of the quadrature operator are as follows

$$|X_\phi, \phi\rangle = \frac{\exp\left[-\frac{1}{2} X_\phi^2 - \frac{1}{2} \mathrm{e}^{2\,\mathrm{i}\,\phi}\, \hat{a}^{\dagger 2} + \sqrt{2} \mathrm{e}^{\mathrm{i}\,\phi} X_\phi\, \hat{a}^\dagger \right]}{\pi^{1/4}} |0\rangle. \tag{4}$$

The total probability distribution must be normalized to one. Hence,

$$\int_{-\infty}^{\infty} \mathrm{d}X_\phi \;\; \omega\left(X_\phi, \phi\right) = 1. \tag{5}$$

2.2. Tomographic entropy

Uncertainties present in the measurements of the physical observables are generally determined by the variances. The alternative approach has been developed using entropic uncertainty relations [31, 32]. The squeezing phenomenon exhibited by the quantum states can be realized by the uncertainty relations and inequalities of entropy [33]. It has been reported that variance-based squeezing is a subset of entropic squeezing [34]. Moreover, the quantum correlations can also be analyzed in terms of entropic relations. For a single mode systems, there exists a significant entropic inequality in terms of position and momentum quadrature of the Shannon information entropy. This inequality gains special attention in the tomographic probability representation. The entropic squeezing of various nonclassical states has been discussed using the Shannon information entropy in the tomographic picture [35–37]. Shannon information entropy in terms of the optical tomogram is represented as

$$S(\phi) = -\int \mathrm{d}X_\phi \;\; \omega\left(X_\phi, \phi\right) \ln\left(\omega\left(X_\phi, \phi\right) \right), \tag{6}$$

$$S(0) = S_x, \tag{7}$$

$$S(\pi/2) = S_y, \tag{8}$$

where S_x and S_y denote the entropy in position and momentum quadrature. The inequality involving the sum of the entropies is defined as

$$S_x + S_y \geq \ln\left(\pi\, \mathrm{e}\right). \tag{9}$$

The state is said to exhibit entropic squeezing if S_x or S_y goes below the value of $\frac{1}{2}\ln(\pi e)$.

3. NSFS with unit quantum efficiency

The optical tomogram of NSFS while using ideal photodetectors in homodyne detection is theoretically evaluated. Then the entropy of the state is numerically computed. Substituting the density operator of the NSFS in (2) results in the expression for the quadrature distribution of NSFS, i.e.,

$$\begin{aligned}\omega(X_\phi, \phi) = \frac{{N_n}^2}{\pi^{1/2}} \Bigg[& |C_n|^2 \mathrm{e}^{-X_\phi^2} \frac{H_n^2(X_\phi)}{2^n\, n!} \\ & - C_n \mathrm{e}^{-\frac{1}{2}|\alpha|^2} \mathrm{e}^{-\left[\frac{1}{\sqrt{2}}|\alpha|\, \mathrm{e}^{-\mathrm{i}\,(\xi-\phi)} - X_\phi\right]^2} \frac{H_n(X_\phi) \mathrm{e}^{-\mathrm{i}\,n\phi}}{\sqrt{2^n\, n!}} \\ & - C_n^* \mathrm{e}^{-\frac{1}{2}|\alpha|^2} \mathrm{e}^{-\left[\frac{1}{\sqrt{2}}|\alpha|\, \mathrm{e}^{\mathrm{i}\,(\xi-\phi)} - X_\phi\right]^2} \frac{H_n(X_\phi) \mathrm{e}^{\mathrm{i}\,n\phi}}{\sqrt{2^n\, n!}} \\ & + \mathrm{e}^{-\left[X_\phi - \sqrt{2}|\alpha| \cos(\xi-\phi)\right]^2} \Bigg]. \end{aligned} \tag{10}$$

Here, $H_n(X_\phi)$ is the Hermite polynomial.

The tomogram pattern of a typical coherent state is identified by the sinusoidal strand (Fig. 1a), while the number state $|n\rangle$ has $n+1$ vertical stripes (Fig. 1b). Figure 1c shows n number of distinct peaks as a result of quantum interference between coherent state and number state, thus manifesting the effects of the state filtration from coherent states. The extent of nonclassicality is observed to be pronounced in the case of filtering number

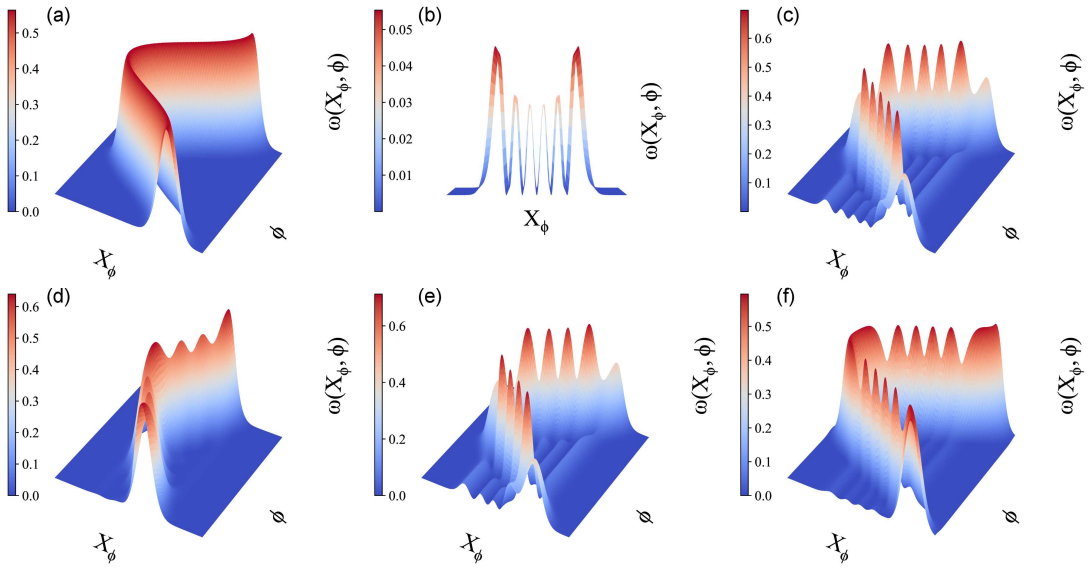

Fig. 1. Panels (a), (b), (c) denote the optical tomogram of coherent state ($|\alpha|^2 = 5$), number state ($n = 5$) and NSFS ($|\alpha|^2 = n = 5$), respectively. Panels (d), (e), (f) show the optical tomogram of NSFS for various coherent amplitudes ($|\alpha|^2 = 1, 4, 8$) and removal of $|4\rangle$ number state.

states from coherent states with appreciable superposition coefficient ($|\alpha|^2 = n$). The optical tomogram of NSFS for various $|\alpha|^2$ and filtration of $|4\rangle$ is plotted in Fig. 1d–f. Either greater or lower case of coherent strength ($|\alpha|^2$) does not capture the distinct view. Peaks are clearly visualized only when the square of the coherent amplitude $|\alpha|$ reaches the value of n — the number state filtered. Since the state is said to exhibit maximum nonclassicality when $|\alpha|^2 = n$, the distinct peaks in the tomogram pattern may be a qualitative indicator of nonclassicality.

From the quadrature probability distribution the Shannon entropy is calculated. The entropic squeezing of the NSFS is illustrated in Fig. 2. Removal of single photon number state $|1\rangle$ makes the entropy of the momentum quadrature S_y to be squeezed in the lower coherent amplitude region. Further removal of successive number state shows the quadrature swap (S_x) and decrease in squeezing. As the choice of the number state $|n\rangle$ to be filtered reaches a higher value, the depth of the squeezing decreases, and squeezing is exhibited for a wider range of the coherent amplitude.

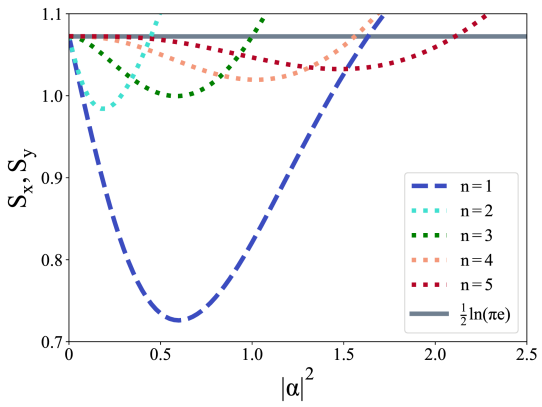

Fig. 2. Existance of entropic squeezing is illustrated for the filtration of $|1\rangle$ to $|5\rangle$ number states for various coherent amplitudes. Dashed line, dotted lines and solid line represent the squeezing in S_y quadrature, squeezing in S_x quadrature and boundary value for the entropic squeezing, respectively.

4. Non-unit quantum efficiency of photodetectors

The non-unit efficiency in photodetection experiments is inevitable. In such experiments, the reconstruction process is not absolute, and hence errors during the experiments have been known to propagate at the time of the reconstruction processes as well. Theoretically, the loss of information in a tomogram pattern can be investigated when efficiency degrades from the maximal level. The effect of detection inefficiency on the tomographic pattern can be examined, and the permissible range of error may be devised with experimental inputs. Using the ideal rotated quadrature probability distribution, the measured quadrature distribution with detection inefficiency is calculated through convolution [38]

$$Pr(q, \phi; \eta) = \frac{1}{\sqrt{\pi\,(1-\eta)}} \int_{-\infty}^{\infty} \mathrm{d}X_\phi\, \omega(X_\phi, \phi) \times \exp\left[-\frac{\eta}{1-\eta}\left(X_\phi - \frac{q}{\sqrt{\eta}}\right)^2\right]. \quad (11)$$

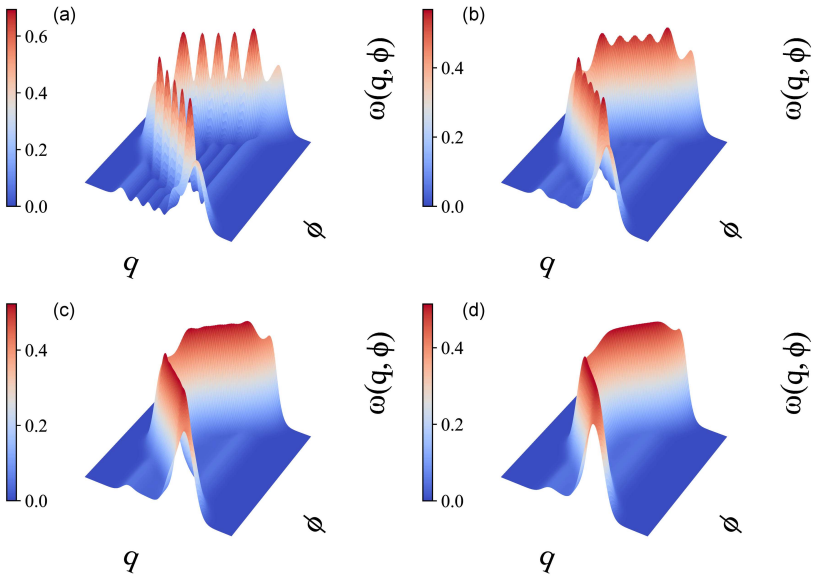

Fig. 3. Degradation of optical tomogram pattern from unit quantum efficiency ($\eta = 1$ (a)) to non-unit quantum efficiency ($\eta = 0.8$ (b), $\eta = 0.6$ (c), $\eta = 0.4$ (d)) for $|\alpha|^2 = n = 5$.

The effect of quantum efficiency on the quadrature distribution of NSFS has been evaluated theoretically and the tomogram pattern is shown in Fig. 3. The computation of the integral (11) is numerically employed and for the unit quantum efficiency ($\eta = 1$), $Pr(q, \phi; \eta)$ retrieves the ideal quadrature distribution $\omega(X_\phi, \phi)$. The number of filtered state is chosen to be equal to the $|\alpha|^2$ value. Figure 3 provides information about the endurance of the nonclassicality and the amplitude of the coherent wave. Initially, with a decrease in η, the recombination of the peaks in the tomogram suggests that the nonclassical properties are getting diminished. It can be observed that there is a decrease in the amplitude of the coherent wave with a reduction in η. However, the sinusoidal strand structure denoting the coherent state remains preserved for $\eta = 0.4$. These observations suggest the effectiveness of filtration in the coherent state.

The stability of the entropic squeezing in the non-unit quantum efficiency is depicted in Fig. 4. The evolution of squeezing for varying coherent amplitude and quantum efficiency is projected in the contour view. The faded area denotes the unsqueezed region, whereas the squeezed area gets dark as the coherent amplitude decreases and the quantum efficiency increases. The entropic squeezing is more robust even in the lower quantum efficiency for the removal of the single photon number state than the five photon number state.

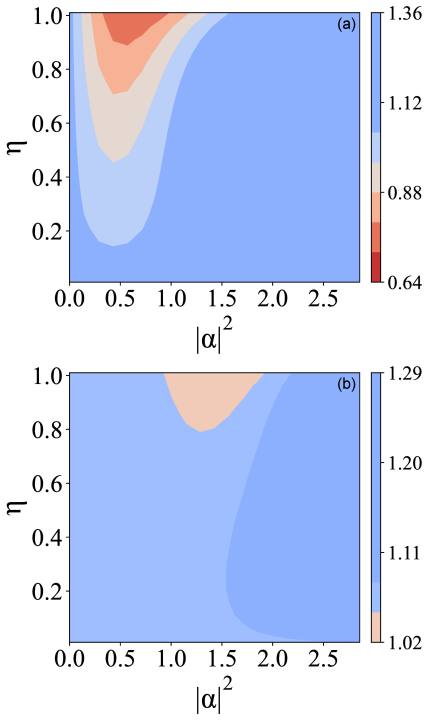

Fig. 4. The contour view of the degradation of entropic squeezing for non-unit quantum efficiency (η) for the removal of $|1\rangle$ (a) and $|5\rangle$ (b) number states. Quadrature S_y (a) and S_x (b) squeezed for the filtration of $|1\rangle$ and $|5\rangle$, respectively.

5. Impact of decoherence

The nonclassical properties of the quantum states deteriorate on interaction with the environment. The decoherence models [39] have been commonly employed in monitoring the extent of nonclassicality in the state. In the following section, the sustainment of the nonclassical nature of NSFS has been analyzed using the phase decoherence model and amplitude decoherence model [40, 41].

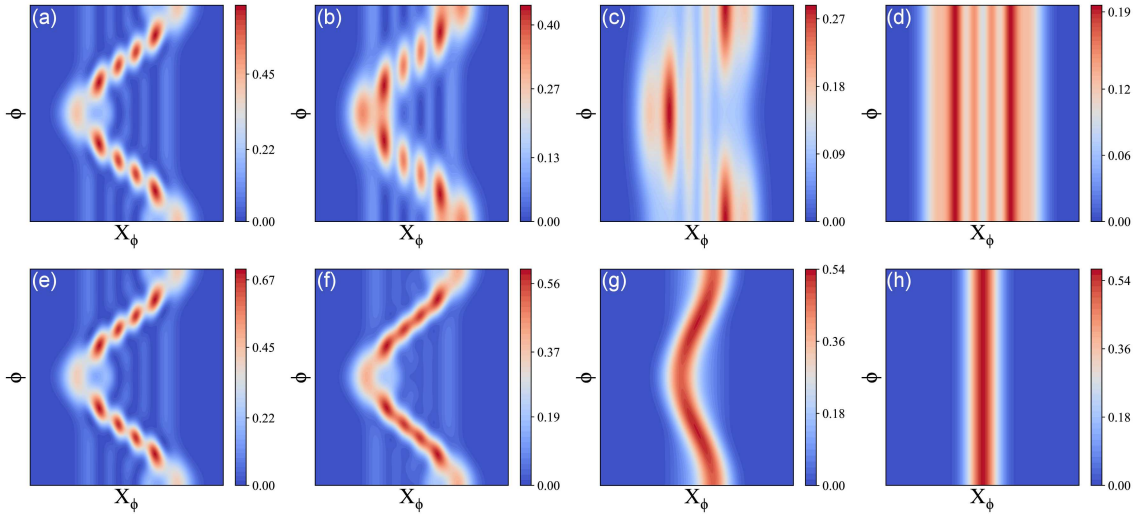

Fig. 5. Evolution of optical tomogram under phase damping (a)–(d) and amplitude damping (e)–(h) models at the given time of $\kappa\tau = \gamma\tau = 0.01$, $\kappa\tau = \gamma\tau = 0.1$, $\kappa\tau = \gamma\tau = 1$, and $\kappa\tau = \gamma\tau = 10$ (right to left) for the state parameter $|\alpha|^2 = n = 4$.

5.1. Phase damping model

The system evolving under this model has been observed to retain the energy of the system, whereas the phase information has been observed to be lost. This can be presented as

$$\hat{H}_{ph} = \sum_{j=0}^{\infty} \hbar\kappa \left(\hat{A}\, \hat{e}_j^{\dagger} + \hat{A}^{\dagger}\, \hat{e}_j \right). \tag{12}$$

Here, $\hat{e}_j$, $\hat{e}_j^{\dagger}$ denotes the environment modes and $\hat{A}$, $\hat{A}^{\dagger}$ indicate the single mode system that has been taken into consideration. The system is coupled to the environment by the coupling constant κ, and the master equation denoting the described system is stated as

$$\frac{\mathrm{d}\hat{\rho}}{\mathrm{d}\tau} = \kappa \left(2\hat{A}\,\hat{\rho}\,\hat{A}^{\dagger} - \hat{A}^{\dagger}\,\hat{A}\,\hat{\rho} - \hat{\rho}\,\hat{A}^{\dagger}\,\hat{A} \right). \tag{13}$$

The time evolved density operator can be written as

$$\hat{\rho}(\tau) = \sum_{u,v=0}^{\infty} \rho_{u,v}(\tau)\, |u\rangle\langle v|. \tag{14}$$

The solution of the master equation is

$$\rho_{u,v}(\tau) = \exp\left[-\kappa (u-v)^2 \tau \right] \rho_{u,v}(\tau = 0). \tag{15}$$

Density operator of NSFS when $\tau = 0$ is represented as

$$\rho_{u,v}(\tau = 0) = N_n^2\, \mathrm{e}^{-|\alpha|^2} \left[\frac{\alpha^u \alpha^{*v}}{\sqrt{u!v!}} - \frac{\alpha^u \alpha^{*n}}{\sqrt{n!u!}} \delta_{n,v} - \frac{\alpha^n \alpha^{*v}}{\sqrt{n!v!}} \delta_{n,u} + \frac{|\alpha|^{2n}}{n!} \delta_{n,u} \delta_{n,v} \right]. \tag{16}$$

Time dependent quadrature distribution under phase damping model is given as

$$\omega(X_\phi, \phi, \tau) = \langle X_\phi, \phi | \hat{\rho}(\tau) | X_\phi, \phi \rangle = \frac{\mathrm{e}^{-X_\phi^2}}{\sqrt{\pi}} \sum_{u,v=0}^{\infty} \rho_{u,v}(\tau) \frac{H_u(X_\phi) H_v(X_\phi)}{\sqrt{2^{(u+v)} u! v!}}\, \mathrm{e}^{-\mathrm{i}(u-v)\phi}. \tag{17}$$

The considered quantum state is pure at $\tau = 0$. The qualitative signatures in the optical tomogram can be monitored by connecting the system to the environment. Figure 5a–d shows the evolution of the tomogram pattern and the distinct rapid oscillations under the phase damping model. The evolution of states at different times ($\kappa\tau = 0.01$, $\kappa\tau = 0.1$, $\kappa\tau = 1.0$, and $\kappa\tau \to \infty$) are captured. It is observed that the state is very robust for $|\alpha|^2 = n$ with the patterns vanishing gradually as shown in Fig. 5b. The distinguished peaks are obtained at the given time of $\kappa\tau = 0.1$, whereas the features weakly decay, retaining the peaks at the curvatures of the sinusoidal strand. As the time approaches infinity, the phase illumination of the state dissipates completely, whereas the particularized form of the decisive mixed state depends on the initial state as shown in Fig. 5d.

5.2. Amplitude decay model

The Hamiltonian corresponding to the reservoir connected to the single mode can be represented using rotating wave approximation as

$$\hat{H}_{\mathrm{amp}} = \sum_{j=0}^{\infty} \hbar\gamma \left(\hat{a}\, \hat{e}_j^{\dagger} + \hat{a}^{\dagger}\, \hat{e}_j \right). \tag{18}$$

The photon numbers have been observed to decrease due to the decay of photons from the system into the reservoir. This effect can be captured using the master equation as

$$\frac{\mathrm{d}\hat{\rho}}{\mathrm{d}\tau} = \gamma \left(2\hat{a}\,\hat{\rho}\,\hat{a}^{\dagger} - \hat{a}^{\dagger}\,\hat{a}\,\hat{\rho} - \hat{\rho}\,\hat{a}^{\dagger}\,\hat{a} \right). \tag{19}$$

The solution for (19) is given as

$$\rho_{l,m}(\tau) = \mathrm{e}^{-\gamma\tau(l+m)} \sum_{k=0}^{\infty} \sqrt{ \left({}^{l+k}C_k \right) \left({}^{m+k}C_k \right) } \times \left(1 - \mathrm{e}^{-2\gamma\tau} \right)^k \rho_{l+k,m+k}(\tau = 0). \tag{20}$$

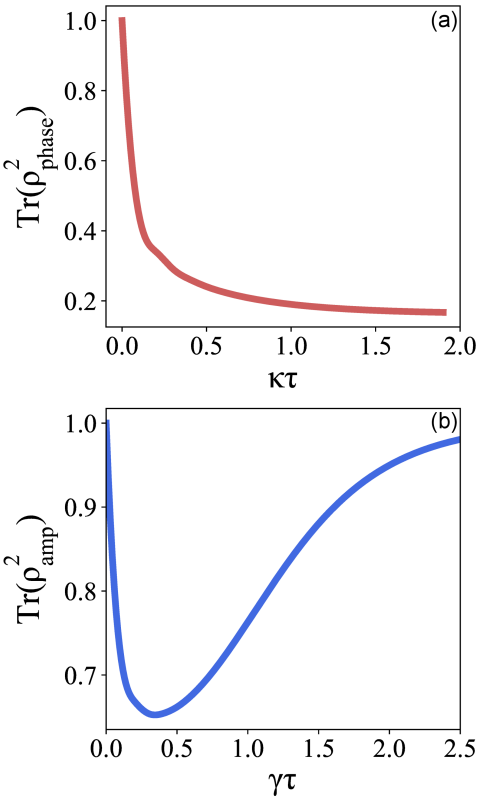

Fig. 6. Purity of the NSFS while evolving in time in (a) the phase damping model and (b) amplitude damping model.

In this section, the duration of the distinct features maintained for the NSFS tomogram is investigated. Figure 5e–h shows the time evolved optical tomogram of NSFS under the amplitude damping model for the coherent amplitude ($|\alpha|^2$) of 4. The coherent amplitude determines the stretch of the sinusoidal strand amplitude in the XY projection of the tomogram. It is observed that the amplitude of the wave decreases with the reduction in photon number as it has been absorbed by the reservoir. As shown in Fig. 5e for ($\gamma\tau = 0.01$), maximum nonclassicality of the state has been emphasized by the recognization of the individual peaks ($\omega(X_\phi, \phi, \tau)$-direction) on the sinusoidal strand rather than the crusts and trough of the strand. The state is capable of maintaining its features for a longer time ($\gamma\tau = 0.1$). It has been observed that with the increase in time ($\gamma\tau = 0.1$), the peaks get fused, denoting the decrease in the nonclassicality and the diminishing nature of the amplitude evidence the reduction in the photon number. In Fig. 5g, the sinusoidal structure has been maintained for ($\gamma\tau$=1.0), owing to its greater coherent strength (α=$\sqrt{4}$). When the state evolves under the amplitude decoherence model for a sufficiently large time ($\gamma\tau \to \infty$), the number of the photons present in the state are completely evacuated and the state becomes the vacuum state. Wherein, information regarding the initial state has been exhausted, attributing to the fact that tomogram of the initial state does not depend on the final state

$$\omega(X_\phi, \phi, \tau \to \infty) = \frac{\mathrm{e}^{-X_\phi^2}}{\sqrt{\pi}}. \tag{21}$$

To describe the evolution of the state under amplitude and phase damping models quantitatively, the purity of the state is calculated, and the results are presented in Fig.6a (phase damping) and Fig. 6b (amplitude damping). A common feature of both evolution models is that the state becomes mixed from the instance when it is connected with the environmental modes. While the evolution under the damping model leads to a completely mixed state at greater periods of time, the purity of the state returns to one in the amplitude damping model since the residual state is the vacuum state. The decay of purity in both models follows a similar pattern. It shows the fragile nature of nonclassicality in the presence of noise.

6. Conclusions

In this work, we have attempted to reveal the imprints of number state filtration from a coherent state in the optical tomogram. Distinct oscillations on the coherent sinusoidal strand are observed as the effect of number state filtration from the coherent state. These oscillations are more pronounced when the number state filtered is matched with the coherent strength ($|\alpha|^2$). These qualitative features exhibited in the optical tomogram are substantiated by calculating the entropic squeezing of the state. The significant squeezing of the Shannon information entropy is achieved for $|\alpha|^2 = n = 1$. To study the effect of experiential imperfections on the evolution of optical tomograms and the subsequent quantities derived from them, the non-unit quantum efficiency of photodetectors is taken into account. The distinct features, such as rapid oscillations on the sinusoidal coherent strand, are shown to be resilient to moderate photodetector quantum efficiencies. Similarly, entropic squeezing is also retained for moderate quantum efficiencies. Further, the robustness of the state is studied by combining the system and environment through phase damping and amplitude damping models, and the subsequent time evolution is captured. It has been shown that the NSFS sustains the oscillations for the special case of mean photon number ($|\alpha|^2$) set equal to the state being filtered (n) for a longer time. Established as a mechanism for inducing nonclassicality in classical states, state filtration is expected to widen the horizon of nonclassical states and their utilization.

Acknowledgments

J. Merlin acknowledges the fellowship and the corresponding author A.B.M. Ahmed acknowledges the financial support of DST-PURSE Phase-II program, Madurai Kamaraj University.

References

[1] U. Fano, *Rev. Mod. Phys*, **29**, 74 (1957).

[2] K.E. Cahill, R.J. Glauber, *Phys. Rev.*, **177**, 1882 (1969).

[3] E. Sudarshan, *Phys. Rev. Lett.* **10**, 277 (1963).

[4] K. Husimi, *Proc. Phys. Math. Soc. Japan* **22**, 264 (1940).

[5] E. Wigner, *Phys. Rev.* **40**, 749 (1932).

[6] A. Ibort, V.I. Man'ko, G. Marmo, A. Simoni, F. Ventriglia, *Phys. Scr.* **79**, 065013 (2009).

[7] K. Vogel, H. Risken, *Phys. Rev. A* **40**, 2847 (1989).

[8] D.T. Smithey, M. Beck, M.G. Raymer, A. Faridani, *Phys. Rev. Lett.* **70**, 1244 (1993).

[9] A.I. Lvovsky, M.G. Raymer, *Rev. Mod. Phys*, **81**, 299 (2009).

[10] A. Ibort, A. Lopez-Yela, *Inverse Probl. Imaging*, **15**, 893 (2021).

[11] G.M. D'Ariano, M. De Laurentis, M.G.A. Paris, A. Porzio, S. Solimeno, *J. Opt. B: Quantum Semiclass. Opt.* **4**, S:127 (2002).

[12] G.M. D'Ariano, M.F. Sacchi, *Phys. Rev. A* **59**, 826 (1999).

[13] M.R. Bazrafkan, V.I. Man'ko, *J. Russ. Laser Res.* **24**, 80 (2003).

[14] S.N. Filippov, V.I. Man'ko, *Phys. Scr.* **83**, 058101 (2011).

[15] Y.A. Korennoy, V.I. Man'ko, *Phys. Rev. A* **83**, 053817 (2011).

[16] R. Schmied, *J. Mod. Opt.* **63**, 1744 (2016).

[17] A. Czerwinski, *Acta Phys. Pol. A* **139**, 164 (2021).

[18] A. Czerwinski, *Acta Phys. Pol. A* **139**, 666 (2021).

[19] J. Szlachetka, A. Czerwinski, *Acta Phys. Pol. A* **140**, 210 (2021).

[20] R.J. Glauber, *Phys. Rev.* **131**, 2766 (1963).

[21] G.S. Agarwal, K. Tara, *Phys. Rev. A* **43**, 492 (1991).

[22] L. Hong, *Phys. Lett. A* **264**, 265 (1999).

[23] A. Zavatta, S. Viciani, M. Bellini, *Science* **306**, 660 (2004).

[24] D.T. Pegg, L.S. Phillips, S.M. Barnett, *Phys. Rev. Lett* **81**, 1604 (1998).

[25] S. Sivakumar, *Int. J. Theor. Phys.* **53**, 1697 (2014).

[26] B. Baseia, M.H.Y. Moussa, V.S. Bagnato, *Phys. Lett A* **240**, 277 (1998).

[27] B. Baseia, J. Malbouisson, *Chin. Phys. Lett. A* **18**, 1467 (2001).

[28] C.C. Gerry, A. Benmoussa, *Phys. Lett. A* **303**, 30 (2002).

[29] N. Meher, S. Sivakumar, *Quantum Inf. Process.* **17**, 233 (2018).

[30] N. Meher, S. Sivakumar, *Quantum Inf. Process.* **19**, 51 (2020).

[31] M.G. Raymer, D.T. Smithey, M. Beck, J. Cooper, *Acta Phys. Pol. A* **86**, 71 (1994).

[32] A. Orlowski, *Phys. Rev. A* **56**, 2545 (1997).

[33] S. De Nicola, R. Fedele, M.A. Man'ko, V.I. Man'ko, *Eur. Phys. J. B* **52**, 191 (2006).

[34] J. Park, J. Lee, H. Nha, *Sci. Rep.* **9** 17835 (2019).

[35] B. Sharmila, K. Saumitran, S. Lakshmibala, V. Balakrishnan, *J. Phys. B-At. Mol. Opt* **50**, 045501 (2017).

[36] P. Laha, S. Lakshmibala, V. Balakrishnan, *J. Mod. Opt.* **65**, 1466 (2018).

[37] S. Iqbal, *J. Russ. Laser Res.* **41**, 451 (2020).

[38] U. Leonhardt, *Measuring the quantum state of light*, Cambridge Univ. Press, Cambridge, (1997).

[39] C.W. Gardiner, P. Zoller, *Quantum Noise*, Springer, Berlin (2004).

[40] A. Biswas, G.S. Agarwal, *Phys. Rev. A* **75**, 032104 (2007).

[41] M. Rohith, C. Sudheesh, *Phys. Rev. A* **92**, 053828 (2015).